Fully inkjet printed gas and humidity CuO sensor on flexible polymer substrate

Ing. Petr Krčmář, Ph.D.

Doctoral Thesis Summary

Tomas Bata University in Zlín

Tomas Bata University in Zlín
Faculty of Technology

Doctoral Thesis Summary

Fully inkjet printed gas and humidity CuO sensor on flexible polymer substrate

Senzor plynů a vlhkosti na bázi CuO připravený výhradně inkoustovým tiskem na ohebném polymerním substrátu

Author: **Ing. Petr Krčmář, Ph.D.**

Study programme: Chemistry and materials technology P2808

Study course: Technology of macromolecular compounds 2808V006

Supervisor: Assoc. Prof. Ing. et Ing. Ivo Kuřitka, Ph.D. et Ph.D.

Consultant: Ing. Pavel Urbánek, Ph.D.

External examiners: Prof. Ing. Jaromír Havlica, DrSc.

Assoc. Prof. Mgr. Aleš Mráček, Ph.D.

Ing. Radka Bálková, Ph.D.

Zlín, June 2019

ACKNOWLEDGEMENT

CONTENT

ABSTRACT

The thesis is concerned with material inkjet printing. The main advantage of this technique is the possibility of use of a wide range of printing liquids (inks). The work focuses on the preparation of inkjet ink based on copper oxide nanoparticles for material printing on flexible polymer substrates and its possible application as a sensor of humidity and volatile organic compounds at room temperature. The ink composition was developed based on the optimization of viscosity and surface tension by the addition of polymeric surfactants. The printing process was optimized with the help of dimensionless criteria and the aid of a drop watch camera system integrated into the used printer, which allows controlling of the ink drop ejection from the nozzle. A standard polyethylene terephthalate (PET) film was selected as the representative substrate used in polymer electronics. Silver nano-ink was used for printing of an interdigitated electrode pattern which was overprinted by the copper oxide ink obtaining thus a flexible flat sensor for detecting alcohol vapours. Printed layers and motives were characterized, and the effectiveness of the prepared sensor was demonstrated by measuring its response to the vapours of water and alcohols. A specific low-temperature sensing mechanism was revealed. Finally, the applicability of prepared sensing devices was demonstrated by fabrication and testing of a sensor field integrating a 3 x 3 matrix of sensing elements.

ABSTRAKT

Předložená práce se zabývá inkoustovým materiálovým tiskem. Hlavní výhoda inkoustového tisku spočívá v možnosti využití širokého spektra inkoustů (roztoky nebo disperse). Práce se soustředí na přípravu inkoustu na bázi oxidu měďnatého pro materiálový tisk na flexibilní polymerní substráty a jeho možné aplikace jako senzoru vlhkosti a par organických látek při pokojové teplotě. Inkoust byl vyvinut na základě optimalizace viskozity a povrchového napětí přidáním polymerních surfaktantů. Proces tisku byl dále optimalizován pomocí bezrozměrných kritérií s využitím řízení tryskání kapek inkoustu při tisku. Substrát z polyetylen tereftalátu (PET) byl vybrán jako nejčastěji používaný v polymerní elektronice. Z inkoustu z nanočástic stříbra vytištěn vzor hřebenových elektrod, a ten byl překryt sensorickou vrstvou s použitím inkoustu z nanočástic oxidu měďnatého, čímž byl vytvořen ohebný senzor. Tištěné vrstvy a motivy na substrátu byly charakterizovány a funkčnost připraveného senzoru byla prokázána měřením odezvy na přítomnost par vody a alkoholů. Byl popsán nízkoteplotní mechanismus funkce senzoru. Aplikační potenciál připravených senzorů byl demonstrován výrobou a testováním pole senzorů integrujícího 3x3 matici senzorických prvků.

1. INTRODUCTION

There are many technologies for the deposition of thin polymer layers. Each method or technique has its specifics, and one of the most widely used methods for the preparation of thin layers from solution is called material printing. Material print allows applying a defined amount of solution precisely to where it is intended by a set rate. For highly viscous liquids (pastes), screen printing is applied. For less viscous liquids, inkjet printing is suitable. Besides bubble, piezoelectric printing is widely used. When an electric voltage is applied to the crystal in the piezoelectric head, the crystal is deformed which causes an increase of the pressure in the capillary; hence a drop of ink is sprayed off the nozzle. Then the voltage is switched off, the crystal returns to its original shape, the head pressure drops, makeup ink and the system is ready to generate another drop. Besides viscosity, surface tension plays a crucial role in forming the droplets. Mechanical ejecting of solution ink droplets operates mostly independently of its chemical composition, which is one of the advantages of this technology. Piezo head works theoretically with any fluid that meets only the viscosity and surface tension as the main processing window criteria. These properties are decisive in the interaction of the deposited liquid volume with the substrate surface as well. However, the real printing process using a specific printing nozzle needs optimization of both the ink and process parameters. Good printability regime may be attained using dimensionless criteria involving whole material-tool-process parameter triade.

The material system of ink and substrate may be adjusted to a large variety of purposes and functions. Therefore, the inkjet printing gets more and more to interest in the field of transparent electronics, sensors and solar cells. Among sensors, there is a lack of cheap, flexible and low temperature operating devices suitable for volatile organic compounds detection. This work is focused on the preparation of flexible sensors based on CuO and on the study of its sensing mechanism at low temperatures.

2. INKJET PRINTING MATERIALS AND PRINTABILITY

It is necessary to distinguish between material that is printed and the material on which is something printed. [1]

2.1 Printing inks

At the present time, there are four main types of inkjet inks available: water-based, phase-change, solvent-based and UV curable. [2] Important ink parameters are the viscosity, surface tension, nature and molecular structure of colourants. Table 1 shows typical parameters of various type of inkjet inks and relevant inkjet printing techniques. [1, 3]

Table 1 The viscosity, surface tension and techniques of inkjet printing typical for various types of inks.[1, 3]

Ink	Viscosity (Pa.s)	Surface tension (Nm^{-1})	Technique*
Water-based	$(1\text{-}5)x10^{-3}$	$(20\text{-}50)x10^{-3}$	PIJ
Phase-change	$(10\text{-}40)x10^{-3}$	$(20\text{-}40)x10^{-3}$	TIJ
Solvent-based	$(2\text{-}10)x10^{-3}$	$(20\text{-}35)x10^{-3}$	DOD PIJ and CIJ
UV curable	$(8\text{-}12)x10^{-3}$	$(20\text{-}30)x10^{-3}$	DOD PIJ

PIJ - piezoelectric inkjet printing, DOD - drop on demand inkjet printing, CIJ - continuous inkjet printing

2.2 Printability of inks

Viscosity and surface tension (surface energy) is considered as the main properties of inks for DOD PIJ. Indeed, producers of inkjet printers (printing heads) define the processing window for the use of their products in terms of viscosity and surface tension ranges applicable at specific fluid ejection (drop) velocities. [4]

2.2.1 Viscosity

Newtonian fluids are defined by Newton's Law:
$$\tau = \eta \cdot \dot{\gamma} \tag{3.1}$$

where τ is the shear stress, η is the shear viscosity and $\dot{\gamma}$ is the shear rate. [5]

Among all models describing time independent fluids, Herschel-Bulkley model can be used for their classification.

$$\tau = \tau_0 + \eta \cdot \dot{\gamma}^n \tag{3.2}$$

where τ is the shear stress; τ_0 is the yield stress; η is the shear viscosity; $\dot{\gamma}$ is the shear rate, and n is the flow behaviour index. [6]

Therefore, the pressure dependence of the viscosity may be neglected in this work. The temperature dependence of the viscosity is most easily expressed according to the Arrhenius relationship.

$$\eta = A e^{\frac{E_a}{RT}} \tag{3.3}$$

Where A is the preexponential factor having the dimension of mPa·s, E_a is the activation energy, T is the thermodynamic temperature, and R is the universal gas constant. [7, 8]

2.2.2 Surface tension

Surface tension (SFT) is the second crucial parameter of inkjet inks. Surface tension is defined as a reversible work necessary for the creation of a unit surface area in a liquid substance. Sometimes it is also called the surface energy, which generalises the concept to solids as well. [7]

Surface tension and interfacial energy play an important role in wetting of the surface of the substrate after the impact of the ink drop. The final shape of a dried material dot, as well as the adhesion of the material, is influenced by the matching of SFT of the ink and surface energy of the substrate. Better wettability could be obtained either by decreasing the surface tension of the ink or by increasing the surface energy of the surface. [8, 9]

2.2.3 Drop generation and dimensionless criteria

The drop generation in DOD PIJ printing process is a repeated cycle process. Each cycle can be described as a sequence of five phases: (1) ejection and stretching of liquid, (2) pinch-off of liquid thread from nozzle exit, (3) contraction of liquid thread, (4) break up of liquid thread into primary drop and satellites, and (5) recombination of primary and satellite drops. Ideally, no break up appears, and spherical drop formation and its travel represent the fourth and last stage. [10, 11] Besides viscosity and surface tension of the ink, inertia and eventually viscoelasticity must be taken into consideration as they influence the final shape and form of the drops too. [12] However, since the breakup of boundary-free Newtonian fluid jets is known very well and is most clearly described historically [13], the analysis of drop generation may be reduced to Newtonian fluid-like model for weakly viscoelastic fluids with a still acceptable level of approximation [10]. Then, the Rayleigh type of axisymmetric varicose instabilities represents an adequate model for drop generation in the inkjet printing process of viscous fluids. [10] The jet breakup theory by Rayleigh estimates the time constant for drop formation. [14]

$$\tau_d = \left(\frac{r_{jet}^3 \cdot \rho}{\sigma} \right)^{1/2} \qquad (3.4)$$

These material, tool and process parameters can be analysed in a scale-independent general manner by a number of their dimensionless groupings – dimensionless numbers, namely by the Reynolds (*Re*), the Weber (*We*), and the Ohnesorge (*Oh*) number. The reciprocal value of the Ohnesorge number is known as the number *Z*. The number Oh^{-2} is known as the Laplace number (*La*) or the Suratman number (*Su*). [15-18]

$$Re = \frac{v \cdot \rho \cdot A}{\eta} \qquad (3.5) \qquad\qquad We = \frac{v^2 \cdot \rho \cdot A}{\sigma} \qquad (3.6)$$

$$Oh = \frac{\sqrt{We}}{Re} = \frac{\eta}{\sqrt{\sigma \cdot \rho \cdot A}} = Z^{-1} \quad (3.7) \qquad La = Oh^{-2} = \frac{Re}{Ca} = \frac{\rho \cdot \sigma \cdot A}{\eta^2} \qquad (3.8)$$

where η, ρ and σ are the dynamic viscosity, the density, and the surface tension of ink respectively, v is the drop velocity, and A is the characteristic length corresponding to the inner equivalent diameter of the nozzle orificium.

The diagram in Figure 1 shows a quadrangle field, in which a fluid is printable and single drop formation may be achieved. Any printable fluid must not be too viscous, i.e. the value of the Ohnesorge number mustn't be higher than 1. On the other hand, if its value is lower than 0.1 satellite drops are formed and the printing process gets progressively worse. This range is actually the same as *Z* values between 1 and 10 (see the paragraph above). The fluid must have sufficient energy for drop formation also which defines the left-lower diagonal borderline from 3 (for *Oh* = 1) to 30 (for *Oh* = 0.1) in Reynolds number space. The right-upper diagonal borderline indicates the splashing onset region from *Re* = 20 (for *Oh* = 1) to *Re* = 130 (for *Oh* = 0.1).
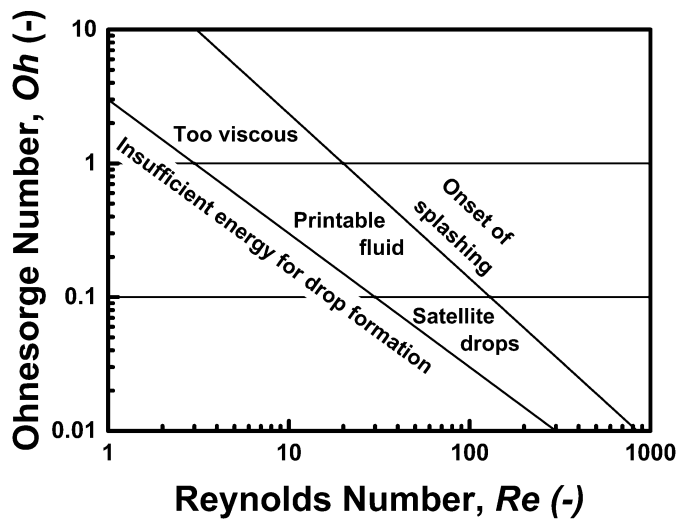

Figure 1 *McKinley & Renardy logarithmic coordinate system, redrawn according to [19].*

The opportunity to revive McKinley-Renardy graph recently published in [20] is used in this dissertation since it covers all material-tool-process parameters also and it offers large ranges of parameters on both axes due to the use of logarithmic scales. Moreover, each value of the Weber number can be represented by a diagonal line with the slope -1 and position according to ist square root because:

$$\log Oh \quad = \quad \log \sqrt{We} - \log Re \quad (3.9)$$

Another approach was developed by Kim&Baek [10]. They identified conditions for a change of drop generation mode, satellite drop formation, satellite recombination with the main drop, and other instabilities or failures in printing. They used the capillary number (Ca) which takes the drop velocity during printing into account although the characteristic length and density are not included and the Weber number which does not contain viscosity.

$$Ca = \frac{We}{Re} = \frac{v \cdot \eta}{\sigma} \quad (3.10)$$

Within these Ca-We coordinates, Kim&Baek mapped various printing regimes including good printability window. The graph is shown in Figure 2. The white area I represents the good printability processing window. Area II covers a field of parameters where one or more satellite drops are generated, but they will not recombine with the main drop. The area III indicates a field of long threads generation which result in fine satellite droplets generation and generally threading due to a simultaneous combination of large Ca and large We. [10]
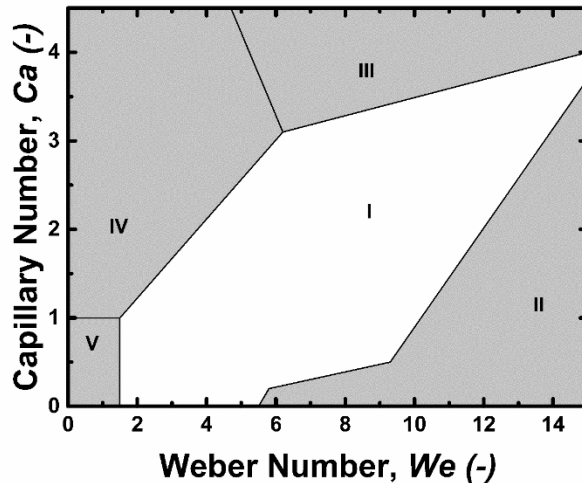
Figure 2 Kim and Baeks Capillary-Weber diagram, redrawn according to [10].

On the other hand, the map in Figure 2 does not include inviscid flows as well as the ink dripping, when the liquid leaks from the nozzles due to week surface tension and low viscosity. Moreover, the range of the x-axis is too small to include printability parameters expressed as We which are advised by the producer of the printer Dimatix used in this study. Pavol Šuly [4] replotted this graph in Re-Ca space and obtained a suitable map covering all possible regimes and failures of inkjet printing. His graph is shown in Figure 3.
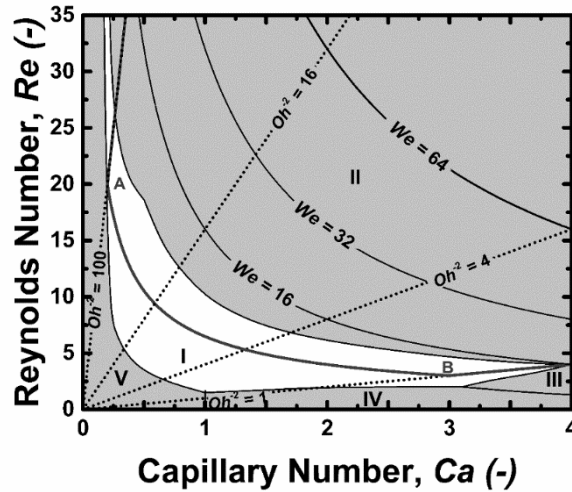
Figure 3 Reynolds-Capillary number diagram, courtesy Pavol Šuly, [4].

2.3 Inks on substrates

The choice of substrate is related to ink selection through maximum processing temperature, spreading, wetting and adhesion interactions, and the requirement for physical flexibility. [2, 21] Another critical step is to achieve matching of the ink surface tension to the surface energy of the substrate. [2]

3. SENSORS

The sensors are defined as the devices which reply to a signal or stimulus and respond with an electrical signal. The signal may be in the form of current, voltage or charge. These stimuli are generally referred to as measurands. The term sensor should be distinguished from the transducer. A transducer is an electronic device that converts energy from one form to another. A sensor is composed of two major components: a sensitive element and a transducer. Figure 4 shows a schematic of a sensor, which incorporates two transducers and direct sensor producing an electrical output. [21-24]
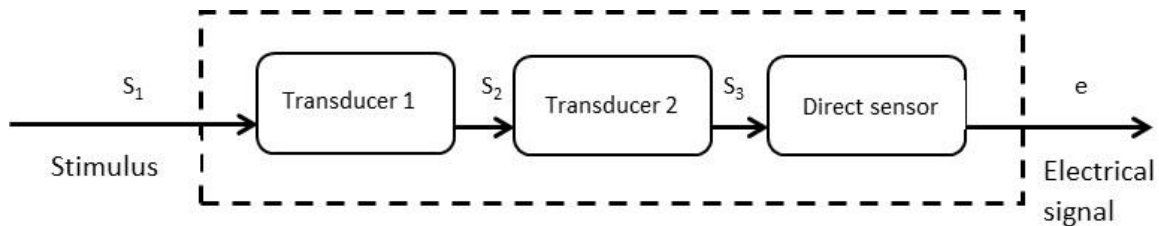
Figure 4 A sensor with two transducers and direct sensor producing electrical output, adapted from [22].

3.1 Sensor for VOC and gases

The detection of such substances is very important in the human environment. Very cheap resistive sensors are popular for such applications, e.g. humidity sensing [25]. They have already introduced many methods of manufacture and methods of measurement that would improve their selectivity and sensitivity under different measurement conditions. [26, 27]

3.2 Sensors based on a change in conductivity

Sensors based on a change in electrical conductivity can be understood as sensors based on changes in electrical resistance also, see Equation 4.3. The electrical resistance can be calculated from Ohm's law (Equation 4.2), but this law applies for direct current only. Changes of external physical, chemical or mechanical properties will change the electrical resistance of the sensor.

$$R = \frac{U}{I} \qquad (4.2) \qquad\qquad G = \frac{1}{R} \qquad (4.3)$$

where R is the electrical resistance [Ω], G is the electrical conductivity [S] = [Ω^{-1}], U is the voltage [V], and I is the electrical current [A].

3.2.1 Resistance measurement

The electrical resistance can be divided according to their size and relevant measurement methods into three categories. A small resistance is a category for $R \leq 1\Omega$, the resistance in the range $1\Omega \leq R \leq 1M\Omega$ are classified as moderate ones, and a resistance higher than $1M\Omega$ is regarded as high. [28-30]

3.3 Printed sensors

The simplest part of the circuit may be formed by just two electrodes contacting an area covered by sensing material layer. (See Figure 5, left side.) In connection with the printed sensors, the term 'interdigit' is often found in the literature. This term refers to most commonly used finger-like electrode pattern, which is formed in a plane two interlocking comb-shaped parallel periodically repeating conductive tracks. [22] Figure 5 shows examples of these patterns of own design.
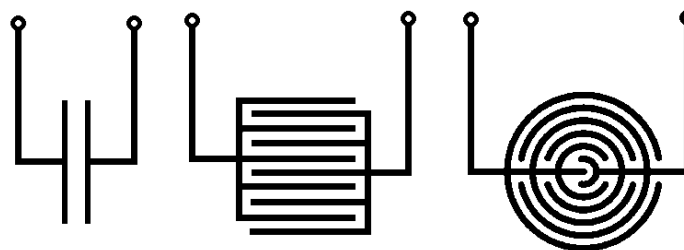

Figure 5 Simplest possible resistance motif – left side. Example of interdigit patterns – the middle and right schematics. [own source]

4. NANOSTRUCTURED CuO FOR SENSORS

Cupric oxide (CuO) has been a hot topic among the studies on transition metal oxide (MO) because of its exciting properties as a p-type semiconductor with a narrow band gap (1.2 eV in bulk) and as the basis of several high-temperature superconductors and giant magneto-resistance materials. [31-39]

4.1 Application in gas sensors

Semiconducting MO gas sensors were firstly introduced in the 1950s when their gas sensitivity at elevated temperature was discovered [40]. Since that time, gas sensors based on these MOs for detection of hazardous, flammable, and toxic gases have been increasingly developed because of their small dimension, low cost, and high compatibility with microelectronic processing. These materials allow fabrication of direct sensors because the response to changing gaseous analyte concentration is a change of the material´s resistivity modulating thus directly the electrical signal. However, these sensors need to be operated at high temperatures usually at least above 200°C to achieve reasonable sensitivity and signal baseline stability [41, 42].

According to the state of the art described, one might consider the field of CuO based sensors being quite well defined and only specific production process and application details remaining open questions. Nevertheless, it pertains the fabrication of high temperature operated sensors only. Preparation of CuO based sensors operating at room temperature is still a challenging issue namely in the form of flexible polymer surface devices which require low-temperature fabrication process also.

5. AIM OF WORK AND OUTLINE OF THE THESIS

The main aim of this Thesis was defined according to the literature review and already gathered experience in our laboratories. The work presented here serves to address specific issues of gas and humidity sensor prepared by inkjet printing on polymer (PET) substrate which requires low-temperature fabrication process and operation of the sensor itself at low temperature as well. In concrete terms, *the aim is to develop and fabricate a novel fully inkjet printed CuO sensor for sensing of alcohol vapours and humidity*. The work shall be done at least to the stage of a proof of concept. It requires the material design of CuO nanostructured particles, formulation of inorganic ink based on nano-CuO for material printing and preparation of a sensor for the detection of alcohol vapours by the material ink-jet printing method. The sensor was tested, and sensing principle of the active material was investigated to identify specific effects connected with the low-temperature preparation and operation of the device.

According to the aim, the objectives of this dissertation are specified as follows:

- Synthesis and characterization of CuO nanostructured particles.

- Preparation and characterization of inorganic ink based on nanostructured CuO particles.

- Sensor design and optimization printing process for prepared ink-jet ink on the material printer (FUJIFILM Dimatix materials Printer DMP-2800 series) and printing of sensors on a selected substrate.

- Characterization of morphology, physical and other properties of printed thin layers as well as the properties of the complete device.

- Testing of prepared sensors for detection of alcoholic vapours and its response to other external conditions and investigation of the sensing mechanism.

- Preparation of a sensor field to demonstrate the capability of the printing process.

6. EXPERIMENTAL

- **Materials**

The aqueous dispersion of Ag nanoparticles (Metalon JS-B25HV, 25 wt%) was delivered by Novacentrix, US. As substrates, PET foils (product name: Novele™ IJ-220 with surface energy 49 mNm^{-1}, thickness 0.15 mm, Bekk smoothness >1000 Sec) were used for material printing and supplied by Novacentrix, US. Finally, both dispersant and stabiliser BYK® 348 and DISPERBYK® 190 were supplied by BYK Additives & Instruments, a member of ALTANA, Germany.

- **Room or laboratory temperature**

Wherever used in this thesis, the room or laboratory temperature means (24±2) °C unless given more precisely. There is air conditioning in the laboratory.

- **Synthesis and characterization of CuO nanoparticles**

CuO nanoparticles were prepared via simple water-ethyleneglycol (water-EG) solvothermal microwave-assisted method. The method was adopted from [43] and enhanced by utilization of microwaves [44]. Cupric chloride dihydrate ($CuCl_2 \cdot 2H_2O$) was used as a precursor. Potassium hydroxide (KOH) was used as a starting agent in the absence of any surfactant or template. All chemicals were of analytical purity and used as received from Sigma-Aldrich s.r.o. The typical experimental procedure was carried out this way: 1 g of $CuCl_2 \cdot 2H_2O$ was dissolved in 54 mL of distilled water. Then, 6 mL of EG and 3 g KOH was added in turns. The as-prepared solution was poured into the Teflon vessel proper to use in the microwave oven (MARS 5, CEM Corporation). Vessels with the solution were sealed to ensure appropriate pressure inside. The reaction was maintained at 100 °C under 110 kPa for 30 minutes. After the reaction, the product was washed by distilled water and absolute ethanol several times to remove eventual impurities. Prepared powder was dried for 20 hours at 60 °C.

Prepared powder was characterized by Scanning electron microscope Nova NanoSEM 450 and by powder X-ray diffraction (XRD) using X'Pert PRO X-ray diffractometer (PANalytical, The Netherlands) with Cu Kα radiation of $\lambda = 0.15406$ nm. The size of nanocrystallite domains was estimated with the help of Scherer equation from the diffraction lines broadening.

- **Ink formulation and its preparation**

The series of inkjet inks were prepared from copper (II) oxide nanoparticles by dispersing them in the mixture of a surfactant and a dispersant in various ratios and constant volume of water. The dispersion process was agitated by an ultrasound apparatus working in 50:50 duty cycle with the full power and 5 minutes (GM 20170, BANDELIN electronic, sonopuls Rosette cell) The concentration of CuO varied in the range of 3-10 wt% and the amount of polymeric dispersant and surfactant was set in the range 5-35 wt%. Five ink compositions were prepared. The viscosity, density and surface tension was measured at 25 °C. Prepared ink compositions and their properties are summarized in Table 2.

- **Determination of crucial ink parameters**

The surface tension measurements were carried out using force tenziometer Krüss K100. The Wilhelmy plate method was used in all cases of determination of surface tension of solutions. The viscosity of dispersions was measured by microviscometer Lovis 2000 M/ME at 25 °C. The diameter of the used capillary tube was 1.8 mm and 1.5 mm for the gold ball. The density was measured by density meter DMA 5000M at 25 °C.

- **Deposition method**

All obtained dispersions were tested for deposition by FUJIFILM Dimatix materials Printer DMP-2800 series. A single square of the size 2 cm x 2 cm was used as the testing motive printed on the PET substrate to evaluate preliminarily the conductivity (by the four-point probe) of inks and silver films. The Ink 4 was found as the best performing for printing and most stable dispersion. Therefore, it was used for the fabrication of sensor devices intended for further testing. The device was fabricated by the same material printer. Interdigitated silver electrode pattern from the commercially available Metalon dispersion was printed on the flexible PET substrate. Printed electrode motives were dried in the vacuum oven at 80 °C for 20 minutes. To achieve a good quality of electrodes, the first layer was trapped by another one under the same conditions. After that, continuous thin CuO film discs were printed on the top of this patterned substrate to form the set of sensing devices. A sheet with printed devices was dried once again under the same conditions as the electrodes. This process was repeated five times to obtain films of sufficient coverage, thickness and quality. Finally, single devices were cut from the printout sheet. Similarly, the sensor field of the 3×3 dimension was manufactured with the use of the same procedure but using a more complex design of printed motif integrating 9 single sensors onto one larger PET sheet.

- **Analysis of printed patterns**

The surfaces of printed patterns were analysed by optical microscope LEICA DVM25000 Digital Camera, Atomic Force Microscopy Dimension ICON in ScanAsyst mode, Scanning electron microscope Nova NanoSEM 450 and optical profilometer Bruker ContourGT.

- **Electrical and sensing properties**

Measurements of printed film conductivity were performed by van der Pauw four-point probe method. The apparatus comprises a Keithley ammeter 6517B, Keithley source 2410, and Keithley switch 7002. The probe contacts were golden coated and square geometry of the samples with contacts joined at the corners was used.

The electrical resistance of the single sensors was measured using multimeter UNI-T HC-UT71D. Figure 6 shows a scheme of prepared gas sensor connected to the resistance meter. The holder with the sensor was quickly transferred into an airtight conical flask full of saturated vapours of the alcohol or water. After 5 min adsorption, the sensor was promptly removed from the flask and for the next 5 minutes the sample was measured in the mode of desorption on the ambient air

atmosphere. Humidity in the laboratory ambient atmosphere was not under control, so it varied naturally over the range of common values and can be a source of baseline drift in records of sensor responses for alcoholic vapours. In the case of humidity sensing, the sensor responses actually to the change between ambient humidity and 100 % RH in saturated vapours. The resistance measurement of each sensor was performed always for three such adsorption-desorption cycles. All measurements were conducted at atmospheric pressure and temperature 25 °C.
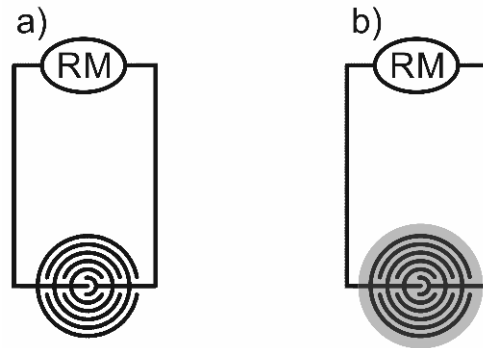

Figure 6 *Schematics of the sensor and its connection in the circuit. RM – resistance meter, a) without sensitive CuO layer and b) with sensitive CuO layer – the grey disk.* *[45]*

Recording of I-V characteristics was performed with the aid of home build setup of a multimeter HP 34401A (Hewlett Packard, USA) utilized for current measurement and a power supply HP 6038A (Hewlett Packard, USA) operated in the regime of voltage control. Both apparatuses were controlled by a PC using Labview application.

All the above described experimental details in this section were published in [45]

The 3 x 3 sensor field (matrix) has one common (ground) conductive path in shape of the outermost loop around the matrix field and 9 measuring channels i.e. one channel for every single device. These are arranged into a flat row of connectors that can be plugged into a female plug a FFC/FPC connector (DS1020-04-22BRT1, CONNFLY). Then, the ground is connected to the 0 th and 10th pin of the connector and the measuring channels are connected to the pins in between. This connector was attached to a Hewlett Packard 34970A multimeter equipped by a 34901A multiplexer module allowing switching between measured channels. The switching frequency was chosen such that a quasi-real time measurement of all 9 channels was made possible, i.e. the sampling frequency of the signal from every sensing element was much higher than its sensing response dynamics. Measured values were recorded by a PC via GPIB (General Purpose Interface Bus). [58]

7. RESULTS AND DISCUSSIONS

In this Thesis, the preparation of fully inkjet printed gas humidity and alcohol vapours CuO based sensor on a common flexible PET substrate is demonstrated. An original microwave-enhanced synthesis of CuO nanostructured particles was developed. Moreover, it is expected that the device should be operated at room temperature. As a proof of application potential of prepared ink and to prepare samples for the study of the sensing mechanism, gas sensors were printed out, characterized and their performance tested.

7.1 CuO particles characterization

In Figure 7, it can be seen that prepared copper oxide nanoparticles have the characteristic morphology of chrysanthemum flowers with a large surface area which gives the best chance of the material to be sensitive to any electron donating gaseous substance. The size of CuO nanosheets which form the individual petals of the flower-like morphology is about several hundred nm in length, the width of the nanosheets ranges from several tens up to one hundred nm and their thickness can be roughly estimated less than a few tens nm. [46, 47]
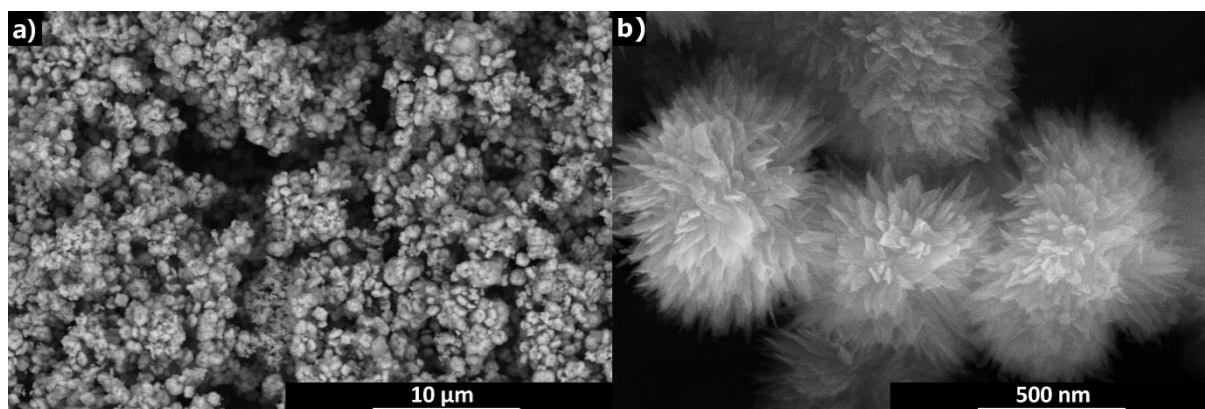
Figure 7 SEM images of CuO nanostructured particles at different magnification. [45]

Results obtained by XRD analysis of prepared powder material are presented in Figure 8. Copper oxide CuO monoclinic phase (C2/c) was confirmed (according to JCPDS No. 01-080-0076) as the prevailing crystalline phase in the material. There are only four peaks of very low intensity in the diffractogram which can be attributed (according to JCPDS No. 01-071-4310) to Cu_2O cubic phase (Pn-3m) manifesting thus the presence of trace concentration of this phase in prepared material. [45]

Figure 8 XRD analysis of prepared powder material. [45]

7.2 Ink formulation and characterization [45]

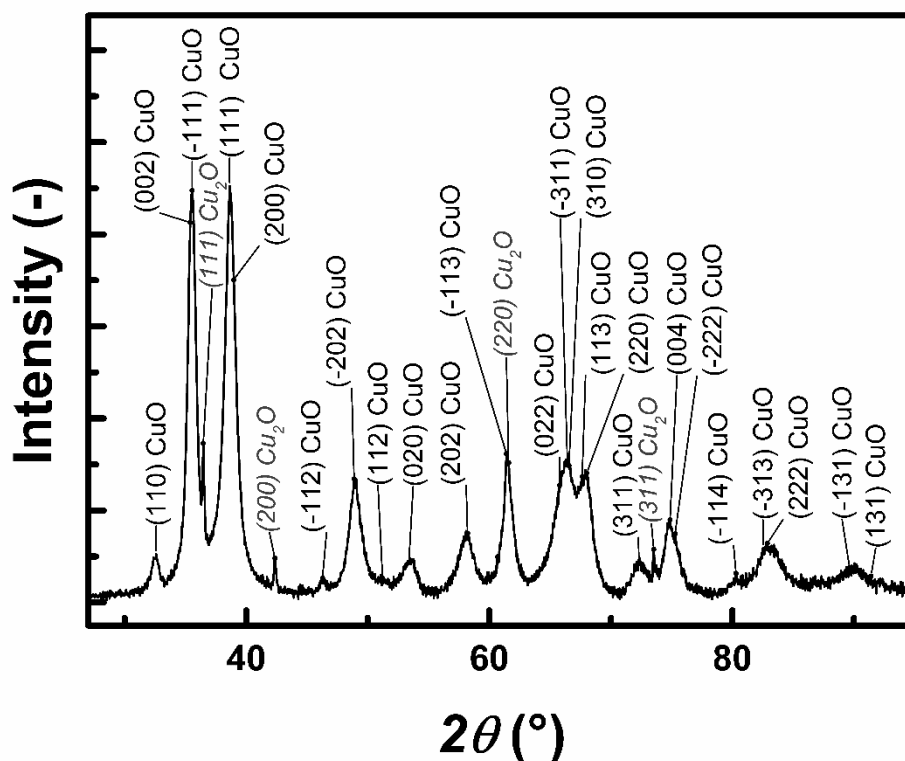**Table 2** shows the experimental values of surface tension and viscosity of prepared CuO inks. The dispersions were prepared at various concentrations of the surfactant and dispersant. As can be seen, additives substantially affect the surface tension in the desired way. These components reduce viscosity, thus the levelling is improved and higher particles loading is possible. Figure 9 illustrates ink sedimentation stability exemplified on an aqueous dispersion of CuO with additives and without additives.

The surface tension of the ink plays an essential role in the formation of droplets and adhesion to the substrate. The surface tension did not significantly vary between different inks and was around 22 mN/m. This is due to the relatively high concentration of additives needed to stabilize the suspensions. Similarly, the density of prepared ink fluids did not vary too. Viscosity was the main parameter varied in dependence on the concentration of solid phase and on the ratio of used surfactant and dispersant additives. [45]

18

Table 2 Composition, viscosity, surface tension and density of CuO ink and solvent at 25°C. [45]

| Ink	Surfactant (wt%)	Dispersant (wt%)	CuO (wt%)	Viscosity (mPa·s)	Surface tension (mN/m)	Density (g·cm^{-3})
Ink 1	21.60	7.20	3.40	(4.66 ± 0.04)	(22.13 ± 0.09)	(1.04±0.04)
Ink 2	14.20	14.20	4.80	(7.13 ± 0.02)	(21.98 ± 0.04)	(1.05±0.06)
Ink 3	13.90	13.90	6.60	(6.53 ± 0.01)	(21.73 ± 0.08)	(1.04±0.03)
Ink 4	7.20	21.60	3.40	(6.59 ± 0.02)	(21.42 ± 0.08)	(1.04±0.07)
Ink 5	12.88	19.32	7.20	(10.54 ± 0.01)	(21.52 ± 0.05)	(1.09±0.04)
Water	0	0	0	(1.00 ± 0.02)	(72.22 ± 0.08)	(0.99±0.01)
CuO + water	0	0	3.00	(1.18 ± 0.02)	(71.56 ± 0.01)	(1.00 ± 0.02)
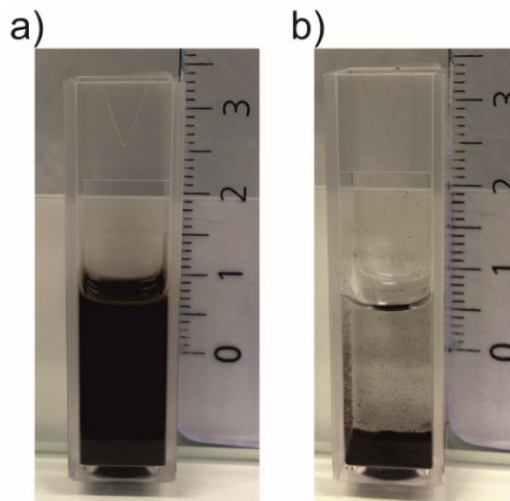
Figure 9 Ink stability of a) aqueous dispersion of CuO with additives after three weeks, and b) aqueous dispersion of CuO without additives after 1 hour. [45]

7.3 Printing process

7.3.1 Preliminary dimensionless criteria analysis

As mentioned in chapter 2.2.3, dimensionless correlations are useful in the development of ink formulation concerning the process conditions and tool used for printing. The graph in Figure 10 constructed according to McKinley and Renardy [19] is used to discuss specific issues of inks [20] prepared in this work. The quadrangle ABCD defines the region where the particular fluids are printable and single drop formation may be achieved or merging with the satellite can be expected.
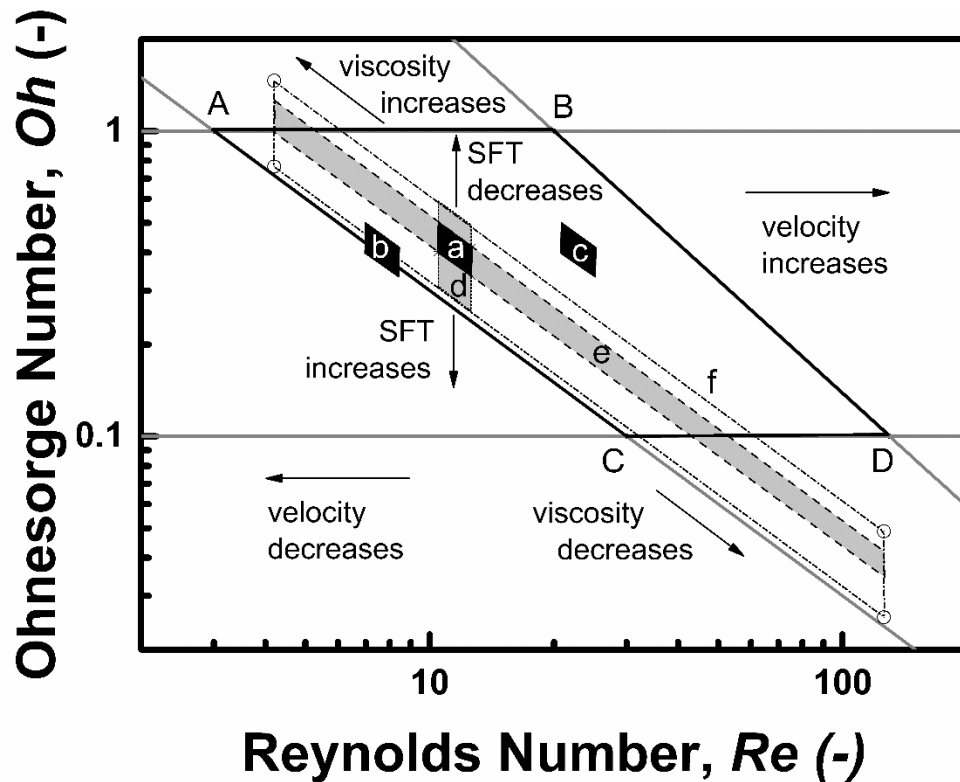
Figure 10 Schematic diagrams showing the operating regime for ink-jet printing according to McKinley and Renardy [19].

The small black parallelogram (**a**) near the centre of the ABCD area represents optimum printability space as defined by the producer for the Dimatix printer at the jetting velocity 6 m/s. The droplet velocity can be varied by the waveform process control (see the next chapter). The small full black parallelograms (**b**) and (**c**) show the printability space of Dimatix printer at jetting velocities 4 and 12 m/s, respectively. Slowing the droplet ejection velocity may be necessary to avoid satellite creation although it can be seen in the graph, that the low velocity can result into failure of drop formation due to the lack of mechanical energy. Hence, the small parallelogram (**a**) is extended into the grey parallelogram (**d**). Increase of the fluid viscosity range from 1 up to 30 mPa·s results into the shift along the top-left to bottom-right diagonal since $Re \sim \eta^{-1}$ and $Oh \sim \eta$ and a slender parallelogram is obtained for this situation denoted as (**e**) with grey filling in the graph. Full extension of the printability span according to both extreme viscosities (1-30 mPa·s) and surface tensions (20-73 mN·m^{-1}) is indicated by the largest quadrangle with circles in its corners and short dash dot sides.

7.3.2 Optimization of printing process

An example of a waveform for CuO ink is given in Figure 11. The most important is to create a perfect waveform, according to this waveform the printhead or more precisely piezoelectric elements operate. Nominally, it is a 10 pL printing head which was used in presented work. However, the actual volume of the drop may be different and was estimated at about 15 pL.

According to preliminary considerations, the velocity about 6 m·s⁻¹ was considered as the first guess, but the conditions were changed according to the analysis described in the following chapter and finally, the velocity of drops was set to 4 m·s⁻¹ to achieve precise drop jetting.

Figure 11 *An example of a waveform which was used for the printing of CuO layers.*
[own source]

7.3.3 Refinement of the dimensionless criteria analysis

Table 3 summarises values of dimensionless criteria calculated for prepared ink dispersions under conditions of the real printing process, i.e. the velocity 4 m/s and characteristic length 21.5 µm of the printing nozzle.

Table 3. Values of selected dimensionless criteria for CuO inks, dispersion of CuO in water and water alone at 25°C based on data from the previous table using the velocity 4 m/s and characteristic length 21.5 µm. [45]

Ink	Dimensionless criterion				
	Re	*We*	*Oh*	*Z*	*Ca*
Ink 1	18.7	15.8	0.212	4.72	0.84
Ink 2	12.4	16.1	0.324	3.09	1.30
Ink 3	13.4	16.1	0.300	3.34	1.20
Ink 4	13.3	16.3	0.305	3.28	1.23
Ink 5	8.7	17.0	0.475	2.11	1.96
Water	83.2	4.6	0.026	38.75	0.06
CuO + water	71.2	4.7	0.030	32.85	0.07

Figure 12 shows positions of prepared inks in the *Oh* versus *Re* space. Tested inks are represented by five empty circle data points labelled following Table 3. Points for water and for CuO dispersion in water are displayed too. It must be

noted, that the points are aligned along a virtual line (marked by a dotted line in the graph), which has the slope -1 representing the constant value of $We^{1/2} = 4$ which corresponds to the average value $We = 16$ from Table 3. Actually, the graph can be parametrised by a set of $We^{1/2}$ isolines based on the formula

$$Oh = \frac{\sqrt{We}}{Re} \qquad (7.1)$$

These hyperbolic isolines transform into straight lines with negative slope using logarithmic axes for plotting *Oh* versus *Re*. The similarity of these lines with diagonal borders of the ABCD area invokes the idea of the importance of the *We* number as discussed in [20]. It can be hypothesised that it is due to the primary importance of surface tension among all discussed inkjet characteristics. The formation of ink droplets is the crucial step of the printing process, and there is only one variable that may work as the source of forces giving the droplet its spherical shape, and it is the surface tension. Indeed, no significant influence of the viscosity was observed, and good printability was achieved by finding the most suitable jetting velocity. [45]
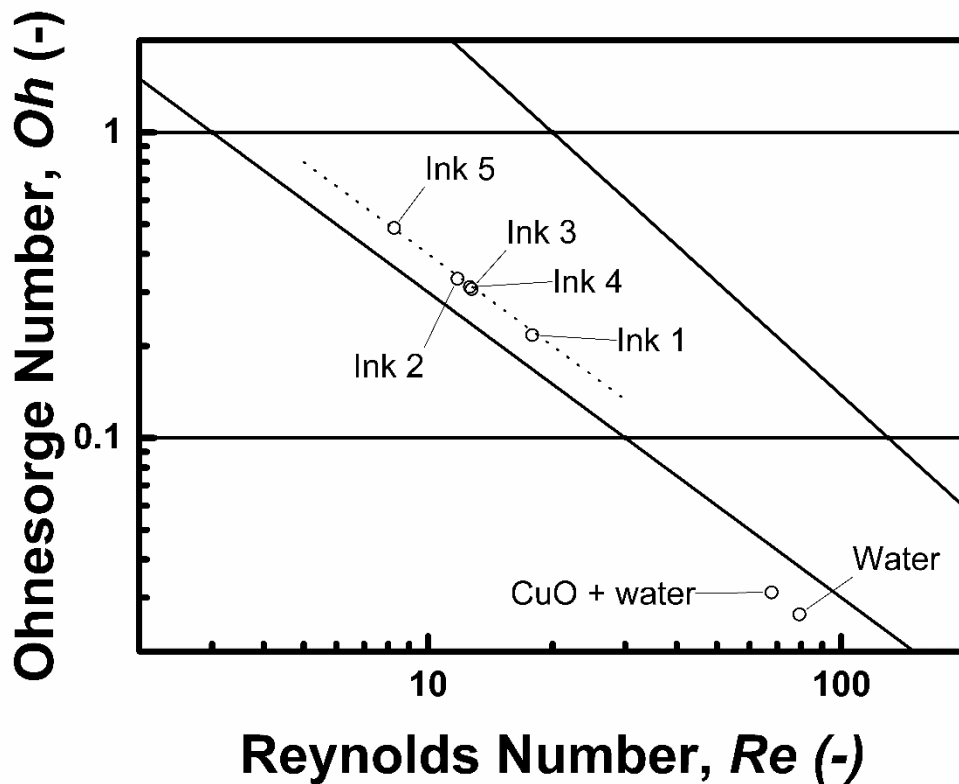

Figure 12 *Positions of prepared inks in the Oh versus Re space.*

A central group of inks (Ink 2, 3 and 4) can be found in the centre of the graph. Nevertheless, the Ink 4 performed better than the Ink 3 under otherwise nearly the same conditions, which points towards the importance of internal material

22

(structural) parameters of the ink. If the fluid is viscoelastic, the elasticity will contribute to the drop formation also, however, more in-depth analysis in that way is beyond the scope of this work and remains as a challenging issue for eventual successors in the research group.
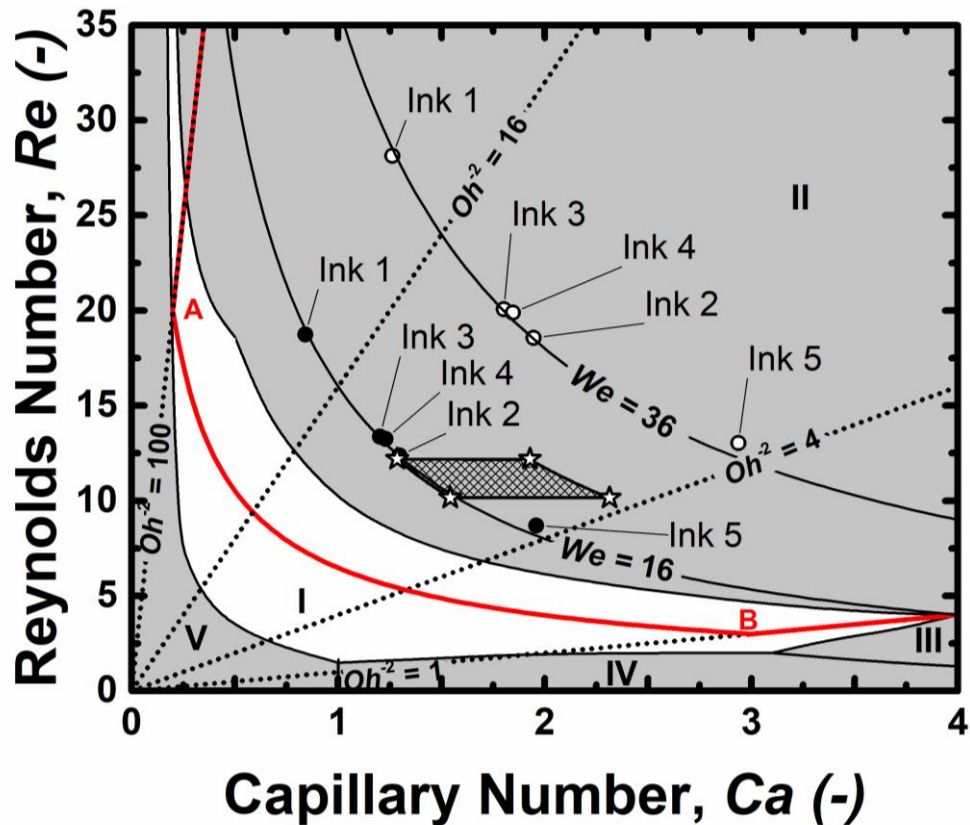

Figure 13 *Processing window for the used printer as suggested by its producer using jetting velocity 6 m/s. [4]*

Since original Kim&Baek's [10] graph for printability assessment is not entirely suitable (see chapter 2.2.3) for systems operating in conditions of higher *We* number, its replotted version may work better [48]. Indeed, the graph in Figure 13 shows the processing window (grey patterned field with empty asterisks in its corners) for the used printer as suggested by its producer using jetting velocity 6 m/s. The meaning of printability areas marked by Roman numerals from I to V is the same as in the original Kim&Baek's publication [10]. The processing window of the printer falls into the area II in which one or more satellite drops are generated, but they do not recombine with the main drop in case of purely Newtonian fluids. However, the excellent printability region I can be expanded towards the top right direction for weakly viscoelastic fluids due to the contribution of elasticity which works in the same direction as surface tension and contributes to recombination of the satellites with the main drop. Operating points for all inks (from Ink 1 to Ink 5) at this velocity are depicted as empty circles aligned along the Weber number isoline at the value 36. It was not possible to

achieve good printability under these conditions. Therefore, the velocity was decreased to 4 m/s, which allowed reasonable printing at *We* = 16. The operating points of inks are plotted as full black circles. The Ink 4 was then found as the best performing among others.

7.3.4 Final tuning of the process parameters

The cartridge temperature 30 °C, a substrate temperature 55-60 °C, and voltage 24 V approximately. The resolution was adjusted to 1280 dpi which corresponds to drop spacing in size of the half dot diameter. The Ink 4 showed good wetting and adhesion to the substrate.

7.4 Analysis of printed patterns – single sensor

The structure of printed Ag layers was analysed microscopically. Figure 14 shows a part of interdigit's surface taken by the optical microscope. The results of SEM observation are shown in Figure 15 in different magnifications.
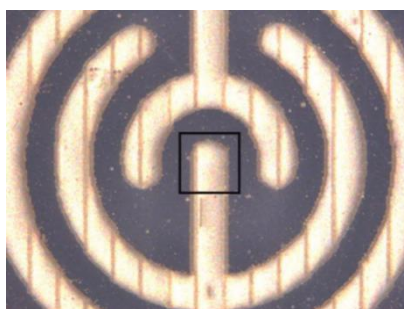

Figure 14 A part of Ag interdigit surface. The black line rectangle in the middle of the image marks the area of the interdigit surface used for further SEM analysis. Image was taken by the optical microscope. [45]

Dimensions of silver particles are below 100 nm. The printed layer was dried at 80 °C in the vacuum to achieve better homogeneity of layers and impart good conductivity to electrodes. It can be seen that there are some macropores in size about 1 μm but they are sparsely distributed that it cannot limit the conductivity of the printed lines of much bigger dimensions. [45]

Sensitive CuO layer was printed on the top of Ag pattern as Figure 16 shows. As can be seen in Figure 17, the CuO layer is relatively compact and the particles kept their original morphology without being either damaged, lost petals or modified in any other way by the processes of ink making and printing. [45]

The sensing layer was printed five times because the trapping of layers improved the coverage, thickness and homogeneity of CuO layer. The AFM measurement confirmed the enormous roughness on nanoscale expected according to the observation of synthesized nanostructured CuO microparticles. The roughness of single CuO layer is 2770 ± 140 nm and of four CuO layers is the roughness 170 ± 70 nm. [45]
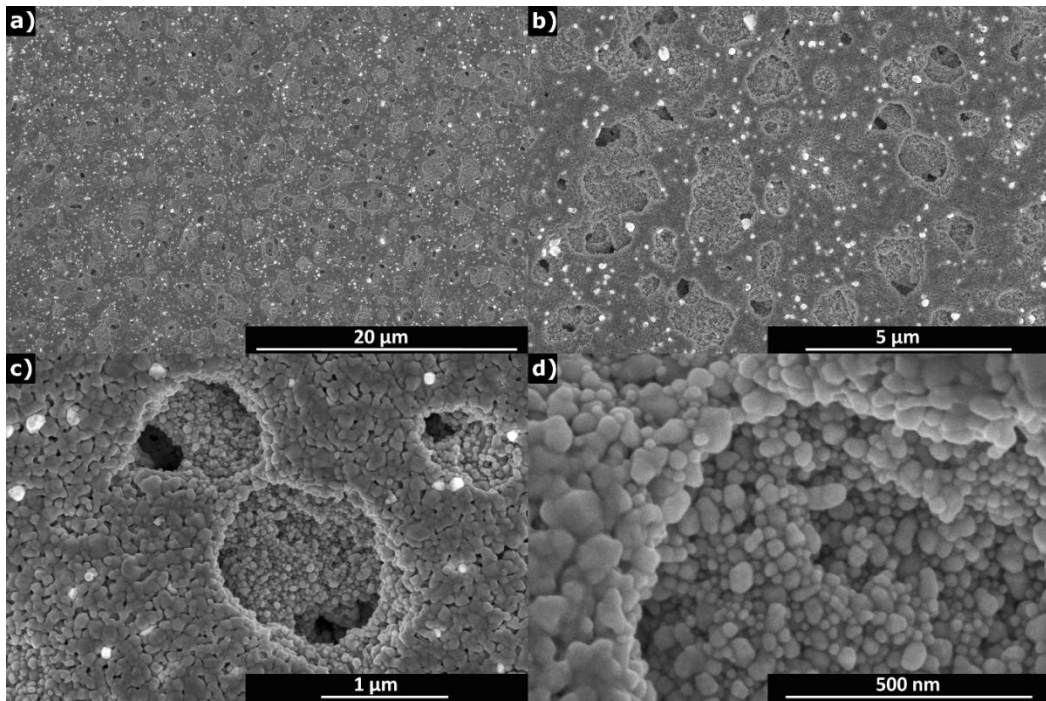
Figure 15 *SEM images of printed Ag layers at different magnification. [45]*
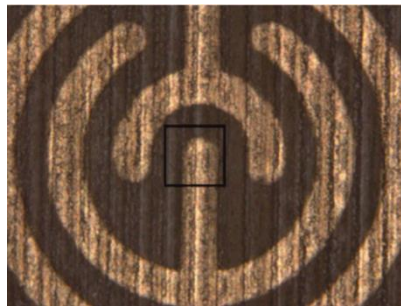

Figure 16 *A part of Ag interdigit with CuO layer surface. The black line rectangle in the middle of the interdigit with CuO layer surface shows the area for SEM analysis. The image was taken by optical microscopy. [45]*
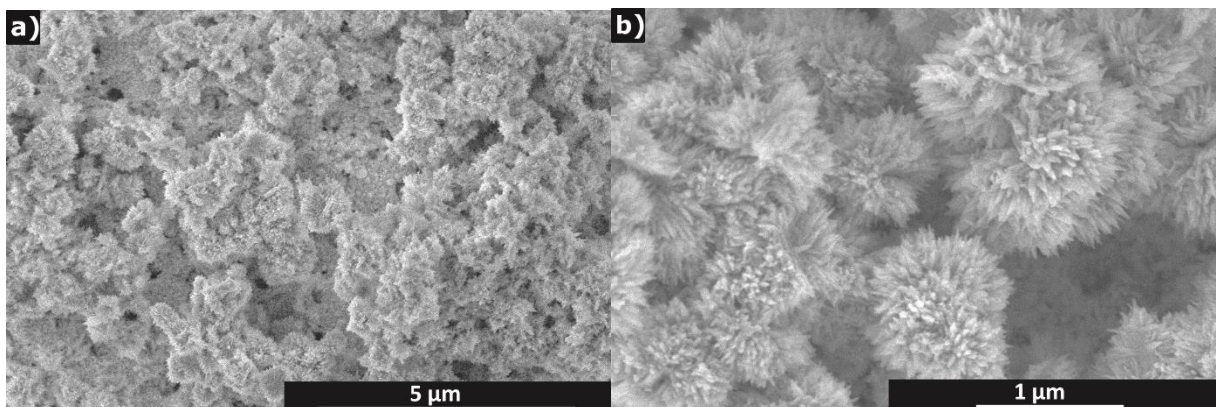

Figure 17 *SEM pictures of printed CuO sensitive layer on Ag layers in different resolution. [45]*

7.5 Resistivity of printed layers

Table 4 shows the conductivities of single-layer material samples deposited on the original substrate and printed with the aim to characterise the basic material components of the multilayer device. The size of the printed square was 2 cm x 2 cm. [49].

Table 4 Resistivity of CuO layer and Ag interdigitate was measured with the four-point probe technique [45]

Material	Resistivity ($\Omega \cdot cm$)
CuO layer (made from Ink 4)	$>10^4$
Ag interdigit	$(2.4 \pm 0.6) \times 10^{-7}$

7.6 Electrical and sensing properties – single sensor

The response and recovery properties of the sensor were investigated first by using ethanol and water as representative examples targeted gas analytes at temperatures 25°C. Firstly, the response of bare interdigitate silver electrode structures was tested. No exposure to any of the tested conditions delivered measurable resistance response. In all cases, overload was signalised by the measuring apparatus indicating thus that the resistance of the incomplete device was higher than 40 MΩ which is the maximum range of the used multimeter. Any contribution of the surface of the flexible PET substrate is excluded. [45]
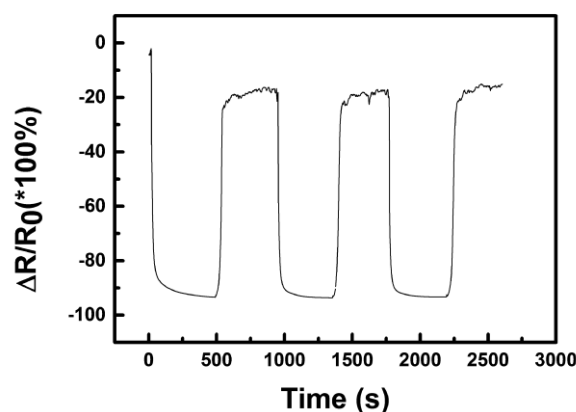

Figure 18 Relative resistance change (ΔR/R0) of the nano-copper oxide sensor within water sensing at 25°C (R – actual resistance value, R0–initial resistance) [45]

Figure 18 shows a typical resistance change of the device prepared with the best ink (Ink 4) composition within the saturated water vapours sensing test at 25°C. The initial value (at time zero) was measured for the sensor freshly taken out from the storage conditions (stored in a desiccator with RH in the range 20-30 %) and it is the first measurable value below the upper measurement range of the multimeter which is 40 MΩ. [45]

The sensing principle of CuO based devices has been numerously reported in [50-52] and many other references. This results in an accumulation of holes at the CuO particle surface while the trapped electrons leave holes following the mechanism [47, 53, 54]:

$$O_2 \leftrightarrow O_2^- + 1hole \tag{7.2}$$

$$\tfrac{1}{2} O_2 \leftrightarrow O^{2-} + VacancyCu^{2+} + 2hole \tag{7.3}$$

Adsorbed molecular oxygen (O_2) can be ionised preferentially to molecular O_2^- at temperatures below 200 °C and to atomic O^- and O^{2-} predominantly at temperatures higher than 200 °C. [45]

When the surface is exposed to water vapour, the doubly ionized oxygen (Equation 7.4) reacts with H^+ coming from the dissociation of water vapour to form OH^- as the below equation [55]:

$$H^+ + O^{2-} \leftrightarrow OH^- \tag{7.4}$$

This reaction leads to the release of the trapped electrons and neutralizes the holes in p-type CuO. Moreover, it can be generalized to any reducing species (such as NH_3 or alcohols etc.) that can be oxidized and release a negative charge (electron). This consequently decreases the concentration of holes and thus increases the resistance in the surface layer of CuO.

Nevertheless, it can be clearly seen in Figure 18 that the resistance of the sensor decreases with increasing humidity which is in opposite to previously described behaviour. It is generally known, that the sensing response is largely influenced by device operating temperature due to the temperature dependence of adsorption-desorption kinetics as well as reaction rates and equilibriums occurring on the sensing material surface. [56, 57]
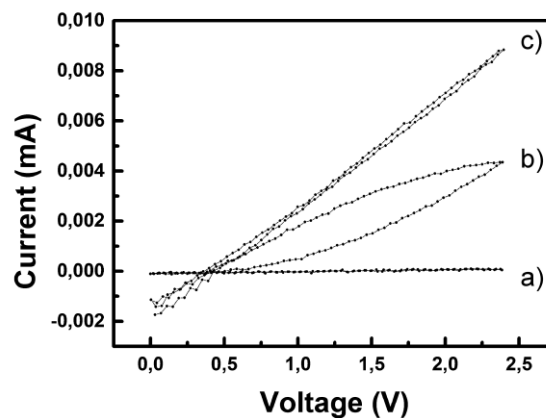

Figure 19 *I-V characteristics of CuO sensors measured at 25°C in water vapours, a) outside from vapours b) hysteresis and c) stabilized. [45]*

In order to investigate this issue, the current-voltage (I-V) characteristics were recorded. Figure 19 shows I−V characteristics of a sample measured at 25°C under three different stages of the testing cycle. Recording of each curve (i.e. from 0 V up to 2.5 V and back down to 0 V) took 60 s. Curve a) was recorded for the

sensor stabilized in the air atmosphere. As can be expected, the resistance of the device is high (calculated from the slope ca 13 MΩ) and there is no hysteresis observed. The second curve b) was recorded for the device after being inserted into the saturated vapour i.e. before the signal saturation. Changing of the resistance value is manifested in a well-developed hysteresis showing a continuous decrease of the resistance of the device. The last curve c) was recorded for the device being equilibrated for five minutes in the saturated vapours. The resistance of the device is obviously stabilized at a constant value and is about 0.2 MΩ (calculated from the slope). The cross-section of the I-V curve with the x-axis was always at about 0.35 V. It must be reminded that the used electrical source was asymmetric (actually not grounded hence floating) and the I-V characteristics were the same regardless to the polarity of the device connection. Indeed, the device is of symmetric design, however, the (0.35 ± 0.02) V offset developed always in the same manner and vanished after the device was taken out from the vapour environment. The value 0.34 V is the standard reduction potential at 25 °C for the following reaction:

$$Cu^{2+}(aq) + 2\,e^- \;\rightarrow\; Cu^0(s) \tag{7.5}$$

As a reasonable explanation can be suggested that an electrochemical cell was temporarily developed each time when the device was exposed to a higher voltage by reduction of a small amount of copper from CuO in vapour environment which created liquid electrolyte environment by condensation in the pores of the sensing layer enabling thus the redox reaction. The Cu phase must be highly dispersed with a large specific surface if created, and oxidized due to oxygen in the air immediately after being removed from the vapour environment and disconnected. Thus we observed the same behaviour in all tests taking the device into the testing chamber and out changing wire connections from time to time. This may have implications towards linearity of the sensor's response in some specific electrical connections (using a higher voltage than the reduction potential for resistance measurement). [45] Similar sets of data were recorded for ethanol and methanol.

7.7 Sensor matrix

The final objective of this Thesis is the preparation of a sensor field to demonstrate the capability of the printing process. Therefore, a flexible device comprising a matrix arrangement of 9 interdigits with sensing function was designed. Its function was demonstrated in its response to alcohol vapours. [58]

7.7.1 Design and preparation of the sensor matrix

Design of the sensor matrix included multiplication of the single interdigit motif described in the chapters above, the arrangement of single devices into a 3 x 3 field and their wiring with a series of conductive paths. [58] The final motif design of conductive paths joining the electrical circuit together is shown in Figure 20.
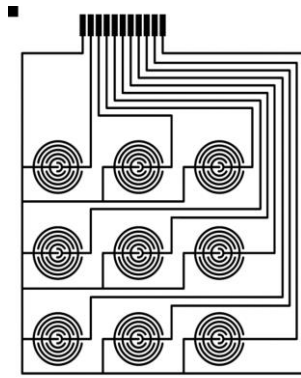
***Figure 20** Motif of conductive paths. Courtesy Petr Měrka, [58]*

The motif for printing sensitive layers was designed so that every single conductive interdigit motive was exactly overprinted by a disc from CuO ink. Prepared motifs were replicated and printed on A4 substrate sheets.

7.7.2 Response of the matrix to alcohol vapours

The data gathered in [58] were further processed and analysed. The adsorption of alcohol vapour molecules causes a sharp decrease of the electrical resistance and their desorption causes a rapid increase of resistance as in the case of single sensing devices. However, the sensor field shows the reproducibility of the effect. The response of the sensor field to a sequence of four exposures to saturated ethanol vapours is shown in Figure 21.
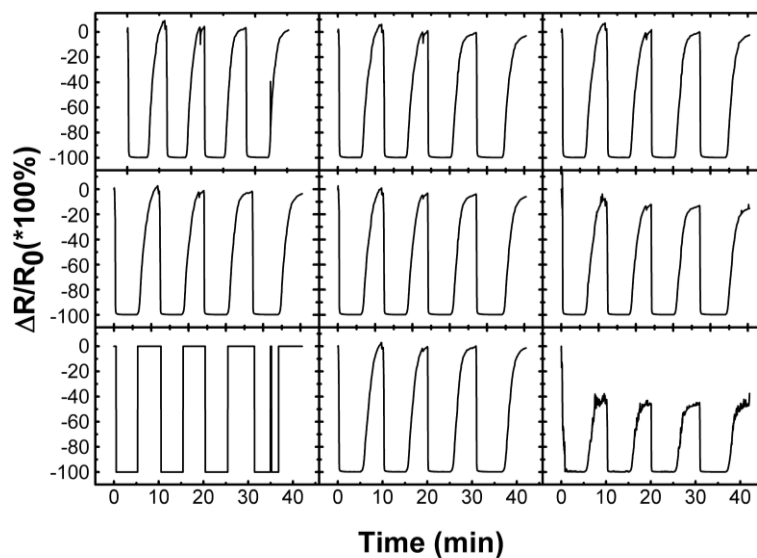

***Figure 21** The response of the sensor field to a sequence of four exposures to saturated ethanol vapours [own source] based on [58].*

To summarize, the potential of preparation of fully printed sensing devices in form of a matrix field on flexible PET substrate was demonstrated and its function with respect to the sensing of alcohol vapours (ethanol, methanol, and isopropanol) was confirmed.

8. CONCLUSIONS

Series of inkjet inks were prepared from copper (II) oxide nanoparticles synthesized by MW enhanced solvothermal technique. The phase structure of prepared powder materials was characterized by XRD technique. An only trace amount of Cu_2O was found in the otherwise prevailing CuO phase. The morphology of prepared particles resembled the shape of chrysanthemum flowers of sub-micrometric size. Anchoring of CuO nanosheets to a common centre like petals in the flower creates large free space between individual nanosheets. Moreover, this expanded configuration of petals is stable and avoids the collapse of the voluminous structure due to the stacking of nanosheets which would occur if exfoliated nanosheets are used and spontaneously assemble during drying of the ink dispersion. This type morphology of constituent blocks of the final sensing layer is suitable for gas sensing purposes.

The particles were dispersed in water with the aid of a mixture of two surface-active compounds (Byk 348 and Disperbyk 190) in different ratio keeping the constant final volume of the dispersion. Dispersions stable over three weeks were prepared. It was found that the addition of a mixture of the dispersant and the stabilizer affects the viscosity of inks more than the content of copper (II) oxide itself. On the other hand, the surface tension of all inkjet inks was around 22 mN·m^{-1} which means that the surface tension of the aqueous dispersion of CuO was reduced more than three times. The viscosity of prepared ink dispersions varied between 4.6 and 10.5 mPa·s. Since the material parameters, namely surface tension, viscosity and density of prepared inks are not sufficient for analysis of their printability, the tool and process parameters were taken into consideration as well. The hydrodynamic diameter of the printing nozzle is the main parameter related to the printer and liquid ejection velocity is the main processing parameter, while the temperature is considered as an external condition. In order to find optimum composition and printing conditions, the printability of inks was analysed in terms of dimensionless criteria. The single criterion approach based on the vast majority of the literature was found insufficient, therefore various two criterial printability assessment approaches were discussed and finally the McKinley & Renardy's map of printability regimes in *Oh* vs. *Re* was revived. This approach was chosen since it utilizes the whole material-tool-process parameter triade and in contrast to other approaches it handles the parametric space within logarithmic coordinates allowing thus investigate and cover a large span of variables influencing the printing process. On the general level, the processing window suggested by the printer producers was analysed with regard to the possibility of good printability achievement. Then, the analytical framework was used in the optimization of the inks and printing process development.

While conductive paths and interdigit electrodes were printed from commercially available silver inks in a standard way, the printing of active layer

from original ink compositions was necessary to optimize. It was possible to achieve good printability with CuO ink drop ejection velocity about 4 m·s⁻¹. First, single thin films were printed to characterize their basic properties, then the CuO active layers were deposited on the electrode patterns to make sensing devices. The trapping of four layers on the primary layer of the CuO improved significantly the homogeneity of the surface as confirmed by the AFM and optical profilometry. The fabrication of the sensing device fully printed on a flexible polymer substrate was finished by posttreatment in a vacuum oven. All processing steps were performed at low temperature limited by the PET substrate stability.

Possible applicability of nanostructured copper (II) oxide films for the methanol, ethanol, and humidity sensing was demonstrated and the sensing mechanism was studied. The operating temperature for sensing was $25\,^{\circ}$C. Good sensitivity and response reversibility of the CuO film-based sensor was proven although no significant differences in selectivity to used alcohols and water were observed. According to the obtained results, the presence of the surfactant and the dispersant remaining in the sensing CuO layer affects its final properties as well as the sensing mechanism. The mechanism typical for p-type of semiconductors was not observed due to the low-temperature operation of the sensor material. A mechanism involving most likely capillary condensation of moisture or vapours in the porous structure of the active layer followed by electrochemical reactions was proposed. An offset about 0.35 V in I-V characteristics of the sensors points towards electrochemical reaction involving the reduction of CuO to Cu^{0}. Also, oxidation of primary alcohols to corresponding aldehydes can be hypothesised as a plausible process influencing the sensing mechanism. Hysteresis was in I-V curves recorded during changes of stimulus concentration as well. Regardless to what is the possible source of sensor's response nonlinearity, it seems that more attention should be paid to the method of resistance measurement itself, namely keeping the voltage applied to the sensor smaller than eventual critical values. [45]

Besides single sensor specimens, the sensor field in the form of a 3 x 3 matrix of single device elements was printed as well. Its function was demonstrated by cyclic exposure to saturated vapours of alcohols, namely ethanol, methanol and isopropanol. Most of the elements showed sufficient reproducibility of the measurements. The selectivity and resistance of printed devices against external conditions remain as the most serious challenges for further research and development.

9. CLOSING REMARKS

9.1 Contribution to science and practice

This work contributed to science and practice by the development of the full inkjet printed gas and humidity CuO based sensor on flexible PET polymer substrate. Moreover, all the partial tasks that had to be researched and developed towards the achievement of the main aim represent a specific contribution in the field of material chemistry and technology:

- A facile microwave assisted the solvothermal method of synthesis of the nanostructured CuO with flower-like morphology suitable for gas sensing was developed.
- Ink formulation and optimization were performed exemplifying good selection of suitable surfactants and stabilizers in order to achieve stable dispersion with suitable surface tension and viscosity.
- Reviving of the McKinley & Renardy's approach to printability regime assessment and good printability parameters evaluation which included a general analysis of the processing window for the used printer. The presented printability analysis framework was used specifically for the laboratory material printer Dimatix DMP 2800 series; however it is applicable to any inkjet printer in a general manner. Similarly, the analysis of ink composition printability emphasizing the Weber number represents a lesson that may be easily adapted to other situations.
- Strong and weak sides of the sensor fabrication at low temperature were demonstrated and discussed.
- Low-temperature sensing mechanism was partially addressed although it partially remains also a question open for further studies. If understood well, it will have implications to further changes in the design of the sensing device.
- Advantages and disadvantages of the resistance measurements with common multimeters were discussed and their consideration resulted into measurements of Volt-Ampere characteristics for each device and analyte application since a sensing device does not necessarily have to be an ohmic element at all.
- Finally, demonstration of the integration of the sensing devices into a sensor field entirely prepared by the inkjet printing confirmed the potential of this technology. On the other hand, future challenges have become evident due to some drawbacks of the prepared specimens.

9.2 Ongoing research and future prospective

The research in the field of printed polymer electronics does not stop with the accomplishment of the aim of this Thesis. Our Group of Multifunctional nanomaterials continues in the research of material properties oriented namely on the understanding structure-property relationship in the active sensing layer

32

materials focusing on the sensing mechanisms under low-temperature operation. Understanding the mechanism will have an impact on the design of the devices which are structures with size-scale dependent properties. With respect to obtained general knowledge, the method of synthesis of nanostructured semiconductor materials will be further developed with the ultimate goal of tailoring desired structure, morphology and function.

Concerning the specific sensors presented in this Thesis, the future research and development will be focused both on the more detailed studies of the sensing mechanism as well as on the issue of the resistance of printed devices against deterioration by external conditions.

REFERENCES

1. LEACH, R.H. *The Printing Ink Manual.* 5th ed. London ; New York: Blueprint, 1993. ISBN 0948905816.

2. MAGDASSI, S. *The Chemistry of Inkjet Inks.* Singapore ; Hackensack, NJ: World Scientific, 2010. ISBN 9789812818218.

3. SOUSA, S., et al. Interactions of Ink Colourants with Chemically Modified Paper Surfaces Concerning Inkjet Print Improvement. *Materials Chemistry and Physics*, MAY 15, 2013, vol. 139, no. 2-3. pp. 877-884 ISSN 0254-0584. DOI 10.1016/j.matchemphys.2013.02.048.

4. ŠULY, P. *Study of Poly(Vinyl alcohol) Solution for Inkjet Printing.* Ph.D. Thesis. ed. Zlin: Tomas Bata University in Zlin, 2017.

5. SOCHI, T. Non-Newtonian Flow in Porous Media. *Polymer*, OCT 15, 2010, vol. 51, no. 22. pp. 5007-5023 ISSN 0032-3861. DOI 10.1016/j.polymer.2010.07.047.

6. SOCHI, T. and BLUNT, M.J. Pore-Scale Network Modeling of Ellis and Herschel-Bulkley Fluids. *Journal of Petroleum Science and Engineering*, FEB, 2008, vol. 60, no. 2. pp. 105-124 ISSN 0920-4105. DOI 10.1016/j.petrol.2007.05.009.

7. SPERLING, L.H. *Introduction to Physical Polymer Science.* 4th ed. New York ; Chichester: Wiley, 2006. ISBN 047170606X.

8. KRONBERG, B., HOLMBERG, K. and LINDMAN, B. *Surface Chemistry of Surfactants and Polymers.* Wiley, 2014. ISBN 9781119961246.

9. STAMM, M. Polymer Surface and Interface Characterization Techniques. *In Polymer surfaces and interfaces: characterization, modification and applications.* M. STAMM ed., 1st ed. Berlin: Springer, 2008., pp. 324 ISBN 9783540738640.

10. KIM, E. and BAEK, J. Numerical Study on the Effects of Non-Dimensional Parameters on Drop-on-Demand Droplet Formation Dynamics and Printability Range in the Up-Scaled Model. *Physics of Fluids*, AUG, 2012, vol. 24, no. 8. pp. 082103 ISSN 1070-6631. DOI 10.1063/1.4742913.

11. DONG, H., CARR, W.W. and MORRIS, J.F. An Experimental Study of Drop-on-Demand Drop Formation. *Physics of Fluids*, JUL, 2006, vol. 18, no. 7. pp. 072102 ISSN 1070-6631. DOI 10.1063/1.2217929.

12. MORRISON, N.F. and HARLEN, O.G. Viscoelasticity in Inkjet Printing. *Rheologica Acta*, JUN, 2010, vol. 49, no. 6. pp. 619-632 ISSN 0035-4511. DOI 10.1007/s00397-009-0419-z.

13. RAYLEIGH, L. On the Instability of Jets. *Proceedings of the London Mathematical Society*, 1878, vol. 1, no. 1. pp. 4-13.

14. HARTMAN, R., et al. Jet Break-Up in Electrohydrodynamic Atomization in the Cone-Jet Mode. *Journal of Aerosol Science*, JAN, 2000, vol. 31, no. 1. pp. 65-95 ISSN 0021-8502. DOI 10.1016/S0021-8502(99)00034-8.

15. JANG, D., KIM, D. and MOON, J. Influence of Fluid Physical Properties on Ink-Jet Printability. *Langmuir*, MAR 3, 2009, vol. 25, no. 5. pp. 2629-2635 ISSN 0743-7463. DOI 10.1021/la900059m.

16. JERRARD, H.G. and MCNEILL, D.B. *A Dictionary of Scientific Units: Including Dimensionless Numbers and Scales.* 6th ed. London ; New York: Chapman & Hall, 1992. ISBN 0412467208.

17. DERBY, B. Inkjet Printing of Functional and Structural Materials: Fluid Property Requirements, Feature Stability, and Resolution. *Annual Review of Materials Research, Vol 40*, 2010, vol. 40. pp. 395-414 ISSN 1531-7331; 978-0-8243-1740-9. DOI 10.1146/annurev-matsci-070909-104502.

18. KUNEŠ, J. and KUNEŠ, J. *Dimensionless Physical Quantities in Science and Engineering.* London ; Waltham, MA: Elsevier, 2012. ISBN 9780124160132.

19. MCKINLEY, G.H. and RENARDY, M. Wolfgang Von Ohnesorge. *Physics of Fluids*, DEC, 2011, vol. 23, no. 12. pp. 127101 ISSN 1070-6631. DOI 10.1063/1.3663616.

20. MASLIK, J., et al. Water-Based Indium Tin Oxide Nanoparticle Ink for Printed Toluene Vapours Sensor Operating at Room Temperature. *Sensors*, OCT, 2018, vol. 18, no. 10. pp. 3246 ISSN 1424-8220. DOI 10.3390/s18103246.

21. *Sensor Technology Handbook.* J.S. WILSON ed., Amsterdam ; Boston: Elsevier, 2005. ISBN 0750677295.

22. FRADEN, J. *Handbook of Modern Sensors: Physics, Designs, and Applications.* 4th ed. New York: Springer, 2010. ISBN 9781441964656.

23. KALANTAR-ZADEH, K. *Sensors: An Introductory Course.* New York: Springer, 2013. ISBN 9781461450511.

24. JANATA, J. *Principles of Chemical Sensors.* Dordrecht ; New York: Springer, 2009. ISBN 9780387699301.

25. CHEN, Z. and LU, C. Humidity Sensors: A Review of Materials and Mechanisms. *Sensor Letters*, DEC, 2005, vol. 3, no. 4. pp. 274-295 ISSN 1546-198X. DOI 10.1166/sl.2005.045.

26. MIELONEN, K., et al. Inkjet Ink Spreading on Polyelectrolyte Multilayers Deposited on Pigment Coated Paper. *Journal of Colloid and Interface Science*,

JAN 15, 2015, vol. 438. pp. 179-190 ISSN 0021-9797. DOI 10.1016/j.jcis.2014.09.077.

27. TITTERINGTON, D.R., BUI, L.V., HIRSCHY, L.M. and FRAME, H.R. *Indirect Printing Process for Applying Selective Phase Change Ink Compositions to Substrates.* 1994 ProQuest Technology Collection.

28. HERRERA, M.A., MATHEW, A.P. and OKSMAN, K. Gas Permeability and Selectivity of Cellulose Nanocrystals Films (Layers) Deposited by Spin Coating. *Carbohydrate Polymers*, NOV 4, 2014, vol. 112. pp. 494-501 ISSN 0144-8617. DOI 10.1016/j.carbpol.2014.06.036.

29. CREGAN, V. and O'BRIEN, S.B.G. Extended Asymptotic Solutions to the Spin-Coating Model with Small Evaporation. *Applied Mathematics and Computation*, OCT 15, 2013, vol. 223. pp. 76-87 ISSN 0096-3003. DOI 10.1016/j.amc.2013.07.071.

30. BANNING, J.H., BUI, L.V., KING, C.R. and TITTERINGTON, D.R. *Phase Change Ink Formulation using a Urethane Isocyanate-Derived Resin and a Urethane Isocyanate-Derived Wax.* 1998 ProQuest Technology Collection.

31. ZHANG, Q., et al. CuO Nanostructures: Synthesis, Characterization, Growth Mechanisms, Fundamental Properties, and Applications. *Progress in Materials Science*, MAR 2014, 2014, vol. 60. pp. 208-337 ISSN 0079-6425. DOI 10.1016/j.pmatsci.2013.09.003.

32. ANANDAN, S. and YANG, S. Emergent Methods to Synthesize and Characterize Semiconductor CuO Nanoparticles with various Morphologies - an Overview. *Journal of Experimental Nanoscience*, 2007, vol. 2, no. 1. pp. 23-56 ISSN 1745-8080. DOI 10.1080/17458080601094421.

33. LIU, Y., et al. Anion-Controlled Construction of CuO Honeycombs and Flowerlike Assemblies on Copper Foils. *Crystal Growth & Design*, MAR, 2007, vol. 7, no. 3. pp. 467-470 ISSN 1528-7483. DOI 10.1021/cg060480r.

34. VASEEM, M., UMAR, A., KIM, S.H. and HAHN, Y. Low-Temperature Synthesis of Flower-Shaped CuO Nanostructures by Solution Process: Formation Mechanism and Structural Properties. *Journal of Physical Chemistry C*, APR 17, 2008, vol. 112, no. 15. pp. 5729-5735 ISSN 1932-7447. DOI 10.1021/jp710358j.

35. MACDONALD, A. Superconductivity - Copper Oxides Get Charged Up. *Nature*, NOV 22, 2001, vol. 414, no. 6862. pp. 409-410 ISSN 0028-0836.

36. R. JANA, et al. *Direct Observation of Re-Entrant Multiferroic CuO at High Pressures.* 2015 Available from Arxiv.

37. XIA, Y., et al. One-Dimensional Nanostructures: Synthesis, Characterization, and Applications. *Advanced Materials*, MAR 4, 2003, vol. 15, no. 5. pp. 353-389 ISSN 0935-9648. DOI 10.1002/adma.200390087.

38. FILIPIC, G. and CVELBAR, U. Copper Oxide Nanowires: A Review of Growth. *Nanotechnology*, MAY 17, 2012, vol. 23, no. 19. pp. 194001 ISSN 0957-4484. DOI 10.1088/0957-4484/23/19/194001.

39. SINGH, D.P. and ALI, N. Synthesis of TiO2 and CuO Nanotubes and Nanowires. *Science of Advanced Materials*, SEP, 2010, vol. 2, no. 3. pp. 295-335 ISSN 1947-2935. DOI 10.1166/sam.2010.1095.

40. POTYRAILO, R.A., SURMAN, C., NAGRAJ, N. and BURNS, A. Materials and Transducers Toward Selective Wireless Gas Sensing. *Chemical Reviews*, NOV, 2011, vol. 111, no. 11. pp. 7315-7354 ISSN 0009-2665. DOI 10.1021/cr2000477.

41. WANG, C., et al. Metal Oxide Gas Sensors: Sensitivity and Influencing Factors. *Sensors*, MAR, 2010, vol. 10, no. 3. pp. 2088-2106 ISSN 1424-8220. DOI 10.3390/s100302088.

42. JIMENEZ-CADENA, G., RIU, J. and RIUS, F.X. Gas Sensors Based on Nanostructured Materials. *Analyst*, 2007, vol. 132, no. 11. pp. 1083-1099 ISSN 0003-2654. DOI 10.1039/b704562j.

43. HONG, J., LI, J. and NI, Y. Urchin-Like CuO Microspheres: Synthesis, Characterization, and Properties. *Journal of Alloys and Compounds*, JUL 29, 2009, vol. 481, no. 1-2. pp. 610-615 ISSN 0925-8388. DOI 10.1016/j.jallcom.2009.03.043.

44. MIRZAEI, A. and NERI, G. Microwave-Assisted Synthesis of Metal Oxide Nanostructures for Gas Sensing Application: A Review. *Sensors and Actuators B-Chemical*, DEC, 2016, vol. 237. pp. 749-775 ISSN 0925-4005. DOI 10.1016/j.snb.2016.06.114.

45. KRCMAR, P., KURITKA, I., MASLIK, J., URBANEK, P., BAZANT, P., MACHOVSKY, M., SULY, P. AND MERKA, P. Fully Inkjet-Printed CuO Sensor on Flexible Polymer Substrate for Alcohol Vapours and Humidity Sensing at Room Temperature. *Sensors*, 2019, vol. 19, no. 14. p. 3068 (20 pp.). ISSN 1234-5678.

46. LUPAN, O., et al. Influence of CuO Nanostructures Morphology on Hydrogen Gas Sensing Performances. *Microelectronic Engineering*, OCT 1, 2016, vol. 164. pp. 63-70 ISSN 0167-9317. DOI 10.1016/j.mee.2016.07.008.

47. CRETU, V., et al. Synthesis, Characterization and DFT Studies of Zinc-Doped Copper Oxide Nanocrystals for Gas Sensing Applications. *Journal of Materials Chemistry A*, 2016, vol. 4, no. 17. pp. 6527-6539 ISSN 2050-7488. DOI 10.1039/c6ta01355d.

48. SULY, P., et al. Poly(Vinyl Alcohol): Formulation of a Polymer Ink for the Patterning of Substrates with a Drop-on-Demand Inkjet Printer. *Materiali in Tehnologije*, 2017, 2017, vol. 51, no. 1. pp. 41-48 ISSN 1580-2949.

49. A.M. HELMENISTINE. *Table of Electrical Resistivity and Conductivity.* ThoughtCo. Sep. 24, 2018, 2018 Available from: https://www.thoughtco.com/table-of-electrical-resistivity-conductivity-608499.

50. HSUEH, H.T., et al. CuO Nanowire-Based Humidity Sensors Prepared on Glass Substrate. *Sensors and Actuators B-Chemical*, AUG 2011, 2011, vol. 156, no. 2. pp. 906-911 ISSN 0925-4005. DOI 10.1016/j.snb.2011.03.004.

51. KIM, H., et al. H2S Gas Sensing Properties of Bare and Pd-Functionalized CuO Nanorods. *Sensors and Actuators B-Chemical*, JAN 3, 2012, vol. 161, no. 1. pp. 594-599 ISSN 0925-4005. DOI 10.1016/j.snb.2011.11.006.

52. HANSEN, B.J., et al. Transport, Analyte Detection, and Opto-Electronic Response of P-Type CuO Nanowires. *Journal of Physical Chemistry C*, FEB 18, 2010, vol. 114, no. 6. pp. 2440-2447 ISSN 1932-7447. DOI 10.1021/jp908850j.

53. WANG, C., et al. Surface Accumulation Conduction Controlled Sensing Characteristic of P-Type CuO Nanorods Induced by Oxygen Adsorption. *Nanotechnology*, APR 11, 2007, vol. 18, no. 14. pp. 145506 ISSN 0957-4484. DOI 10.1088/0957-4484/18/14/145506.

54. LI, D., HU, J., WU, R. and LU, J.G. Conductometric Chemical Sensor Based on Individual CuO Nanowires. *Nanotechnology*, DEC 3, 2010, vol. 21, no. 48. pp. 485502 ISSN 0957-4484. DOI 10.1088/0957-4484/21/48/485502.

55. CHAUHAN, P., ANNAPOORNI, S. and TRIKHA, S. Humidity-Sensing Properties of Nanocrystalline Haematite Thin Films Prepared by Sol-Gel Processing. *Thin Solid Films*, JUN 1, 1999, vol. 346, no. 1-2. pp. 266-268 ISSN 0040-6090. DOI 10.1016/S0040-6090(98)01771-4.

56. PITOIS, A., PILENGA, A., PFRANG, A. and TSOTRIDIS, G. Temperature-Dependent CO Desorption Kinetics on Supported Gold Nanoparticles: Relevance to Clean Hydrogen Production and Fuel Cell Systems. *International Journal of Hydrogen Energy*, APR, 2011, vol. 36, no. 7. pp. 4375-4385 ISSN 0360-3199. DOI 10.1016/j.ijhydene.2010.12.123.

57. TANVIR, N.B., YURCHENKO, O., LAUBENDER, E. and URBAN, G. Investigation of Low Temperature Effects on Work Function Based CO2 Gas Sensing of Nanoparticulate CuO Films. *Sensors and Actuators B-Chemical*, AUG, 2017, vol. 247. pp. 968-974 ISSN 0925-4005. DOI 10.1016/j.snb.2017.11.020.

58. MĚRKA, P. *Matrix Element for Sensors Printed on Flexible Substrate.* MSc. Thesis ed. Zlin: Tomas Bata University in Zlin, 2015.

LIST OF FIGURES

LIST OF TABLES

LIST OF ABBREVIATIONS

3D   three-dimensional
AFM atomic force microscopy
CB   conduction band
CIJ   continuous inkjet
CMC critical micelle concentration
DOD Drop-on-Demand
DPI   Dots per inch
EM   energetic material
GPIB General Purpose Interface Bus
ITO   Indium tin oxide
MO   Metal oxide
MSD Minimum stand-off distance
MW microwave
LIB   lithium-ion batterie
LSDA local spin-density approximation
PC   Polycarbonate
PCB Printed circuit boards
PE   Polyethylene
PES Polyester
PET Poly(ethylene terephthalate)
PI   Polyimide
PIJ   Piezoelectric inkjet
PP   Polypropylene
PS   Polystyren
PTFE Polytetrafluoroethylene
PVC Polyvinylchlorid
PZE Piezoelectric element
RFID Radio-frequency identification
SEM scanning electron microscope
SFT Surface tension
TIJ   Thermal inkjet
UV   Ultraviolet
VB   valence band
VOC Volatile organic compound
XRD X-ray diffraction

LIST OF SYMBOLS

A Preexponential factor
B Sensitivity
E_a Activation energy
R   Universal gas constant
R *electrical resistence*
$R0$ *initial resistance*
U *voltage*
I *electrical current*
T   Thermodynamic temperature
S *Electrical conductivity*
S   Response electrical signal
s   Stimulus
wt% percentage by mass
τ Shear stress
η Shear viscosity
$\dot{\gamma}$ Shear rate
r radius
ρ Density
σ Surface tension
τ_d Time constant
τ_0 Yield stress
v Velocity
n Flow behaviour index
λ wavelength

LIST OF UNITS

°C   degree Celsius

A   ampere

cm   centimeter

eV   electronvolt

g   gram

g·cm⁻³ gram per reciprocal cubic centimeter

h   hour

kPa   kilopascal

m/s   meter per reciprocal second

min   minute

mm   milimeter

ml   mililiter

mN/m   milliNewtons per meter

mPa·s   milliPascal second

nm   nanometer

Pa   Pascal

pL   picoliter

S/m   siemens per meter

s⁻¹   reciprocal second

Ω   Ohm

Ω·cm Ohm centimeter

Ω⁻¹   reciprocal Ohm

kΩ   kiloOhm

MΩ   megaOhm

V   volt

μm   micrometer

LIST OF DIMENSIONLESS NUMBERS

Ca   Capillary number

La   Laplace number

Oh   Ohnesorge number

Re   Reynolds number

Su   Suratman number

We   Weber number

Z   Z number, reciprocal Ohnesorge number

LIST OF PUBLICATIONS AND OTHER OUTPUTS

Articles available in WoS

1. P. Suly, P. Krcmar, J. Maslik, P. Urbanek, I. Kuritka, Poly(vinyl Alcohol): Formulation of a Polymer Ink for the Patterning of Substrates with a Drop-On-Demand Inkjet Printer, Materiali in Tehnologije. 51 (2017) 41-48.

2. J. Matyas, L. Munster, R. Olejnik, K. Vlcek, P. Slobodian, P. Krcmar, P. Urbanek, I. Kuritka, Antenna of silver nanoparticles mounted on a flexible polymer substrate constructed using inkjet print technology, Japanese Journal of Applied Physics. 55 (2016) 02BB13.

3. J. Maslik, I. Kuritka, P. Urbanek, P. Krcmar, P. Suly, M. Masar, M. Machovsky, Water-Based Indium Tin Oxide Nanoparticle Ink for Printed Toluene Vapours Sensor Operating at Room Temperature, Sensors. 18 (2018) 3246.

Submitted manuscript

4. P. Krcmar, I. Kuritka, J. Maslik, P. Urbanek, P. Bazant, M. Machovsky, P. Suly, P. Merka, Fully Inkjet-Printed CuO Sensor on Flexible Polymer Substrate for Alcohol Vapours and Humidity Sensing at Room Temperature. Sensors, 2019, submitted before the submission of the dissertation. ISSN 1234-5678. Published on 11th July 2019. See the reference number [45].

Conference proceedings in WoS

5. P. Urbanek, I. Kuritka, P. Krcmar, J. Maslik, J. Bartos, Polysilanes Thin Films Doped by Coumarin, Nanocon 2012, 4th Internat. Conf. (2012) 391-394.

6. P. Krcmar, P. Urbanek, I. Kuritka, J. Maslik, J. Bartos, The Effect of the Exalite Dopant on Photoluminescence of Poly[methylphenylsilane] in Thin Films, Nanocon 2012, 4th Internat. Conf. (2012) 832-835.

7. J. Matyas, R. Olejnik, P. Slobodian, L. Munster, P. Krcmar, A. Steininger, Multiband Antenna made of Flexible Polymer Substrate Printed with Silver Nanoparticles using Inkjet Print Technology - a Feasibility Study, Nanocon 2015: 7th Internat. Conf. (2015) 377-381.

Other conference proceedings

8. Petr Krčmář, Pavel Urbánek, Ivo Kuřitka. The influence of the substrate surface on deposition of thin layers from PEDOT:PSS. In Plastko 2012 Conference proceedings, 2012 ISBN 978-80-7554-137-7

9. Petr Krčmář, Pavel Urbánek, Ivo Kuřitka, Jan Mašlík and Pavol Šuly (2014), The preparation and characterization of CuO inkjet inks for gas sensors. Lopec

2014 7th International Exhibition and Conference for the Printed Electronics Industry – Conference proceedings

10. Jan Mašlík, Pavel Urbánek, Ivo Kuřitka, Petr Krčmář, Pavol Šuly and Michal Machovský (2014), The preparation and characterization of ITO ink for gas sensing. Lopec 2014 7th International Exhibition and Conference for the Printed Electronics Industry – Conference proceedings

11. Jan Maslik, Pavel Urbanek, Ivo Kuritka, Petr Krcmar; Surface Modification of ITO coated PET foil for material printing. Conference contribution for Eurodisplay 2013 ISSN: 2168-0159

12. Pavel Urbanek, Ivo Kuritka, Petr Krcmar, Jan Maslik; Optoelectronic properties of MEH-PPV thin films influenced by their thickness. Conference contribution for Eurodisplay 2013 ISSN: 2168-0159

13. Pavel Urbánek, Ivo Kuřitka, and Petr Krčmář. 2011. The Influence of ZnO content on optoelectronic properties of films from MEH-PPV/ZnO composite. In Proceedings of MACMESE'11. WSEAS, Stevens Point, Wisconsin, USA, 411-414, ISBN: 978-1-61804-046-6.

Patents and patent applications

14. Active layer for electroluminescent foils. Ivo Kuřitka, Pavel Urbánek, Petr Krčmář, Mráček Jakub. ID 304387-Patent

15. Inorganic ink for material printing applications, comprises copper oxide nanoparticles, polymeric dispersant and rest of water. Krčmář, P, Kuřitka, I, Mašlík J, Šuly P, Urbánek P. ID 307435-Patent

Utility models

16. Inorganic ink based on nanoparticles, intended especially for material printing. Ivo Kuřitka, Pavel Urbánek, Petr Krčmář, Jan Mašlík, Pavol Šuly. ID 26391- Utility model

17. Polymeric ink for material printing. Ivo Kuřitka, Pavel Urbánek, Petr Krčmář, Jan Mašlík. ID 26729-Utility model

18. Active layer for electroluminescent foils. Ivo Kuřitka, Pavel Urbánek, Petr Krčmář, Mráček Jakub. ID 25048-Utility model

Proofs of concept

19. Printed flexible sensor for gas detection. Ivo Kuřitka, Pavel Urbánek, Petr Krčmář, Jan Mašlík. ID 43871727-Proof of concept

20. Printed flexible thermo sensor. Ivo Kuřitka, Pavel Urbánek, Petr Krčmář, Jan Mašlík. ID 43871728- Proof of concept

CURRICULUM VITAE

Petr Krčmář

born in Zlín, Czech Republic, 1986, August 03

Permanent address: Sadová 1027, Valašsské Klobouky 766 01

Phone: (+420)-57-603-8128

Email: pkrcmar@ft.utb.cz

Employment: 2015-2018 ZÁLESÍ a.s., Uherskobrodská 119, 763 26 Luhačovice

Education: 2011-2019: Faculty of technology, Tomas Bata University in Zlin, Czech Republic, Ph.D. degree in Technology of Macromolecular compounds.

2009-2011: Faculty of technology, Tomas Bata University in Zlin, Czech Republic, Master´s degree Ing. (MSc.) in Polymer Engineering.

2006-2009: Faculty of technology, Tomas Bata University in Zlin, Czech Republic, Bachelor´s degree Bc. (BSc.) in Chemistry and Materials Technology.

Projects:

FR-TI3/424 The electroluminescence foils for safety interior lighting – Member of the project team

IGA/FT/2014/006 *The modification of polymer substrates and new materials for inkjet printing of sensors* - member of research team

IGA/FT/2013/025 *The material printing of polymeric and inorganic inks for advanced applications* - member of research team

IGA/FT/2012/025 *The modified polymeric materials for thin layers* - member of research team

Petr Krčmář

Fully inkjet printed gas and humidity CuO sensor on flexible polymer substrate

Senzor plynů a vlhkosti na bázi CuO připravený výhradně inkoustovým tiskem na ohebném polymerním substrátu

Doctoral Thesis Summary